Microchimica Acta (2024) 191:120
https://doi.org/10.1007/s00604-024-06196-5

ORIGINAL PAPER

# Bi-functionality of glyoxal caged nucleic acid coupled with CRISPR/Cas12a system for $Hg^{2+}$ determination

Ying Yu[1] · Yuan Zhang[2] · Xu Chen[2] · Wenhui Li[3] · Zhengwu Wang[3] · Qin Mi[4] · Juan Zhang[2]

Received: 19 October 2023 / Accepted: 6 January 2024 / Published online: 1 February 2024


## Abstract

A highly sensitive and selective fluorescence method has been conducted for the detection of $Hg^{2+}$ based on aminophenylboronic acid–modified carboxyl magnetic beads (CMB@APBA) and CRISPR/Cas12a system mediated by glyoxal caged nucleic acid (gcDNA). As a bi-functional DNA linker, gcDNA offers advantages of simultaneous recognition by boronic acid and complementary DNA/RNA. Under acidic condition, gcDNA can be immobilized on CMB@APBA through the formation of borate ester bond. The formed boric acid–esterified gcDNA can further bind with complementary CRISPR RNA through A-T base pairing to activate Cas12a with $k_{cat}/K_m$ ratio of $3.4 \times 10^7$ $s^{-1}$ $M^{-1}$, allowing for amplified signal. $Hg^{2+}$ can specifically combine with CMB@APBA, resulting in the release of gcDNA from CMB@APBA and the following inhibition on the activation of CRISPR/Cas12a system around magnetic bead. Under optimal conditions, the method exhibits a linear range from 20 to 250 nM, with a detection limit of 2.72 nM. The proposed method can detect $Hg^{2+}$ in milk and tea beverages, providing a great significance for on-site monitoring of $Hg^{2+}$ contamination in food.

**Keywords** Glyoxal caged nucleic acid · Bi-functional linker · Boronic acid; Modified magnetic beads · CRISPR/Cas12a; Fluorescence detection · $Hg^{2+}$

## Introduction

Bi-functional linker plays a key role for the design of detection method and the construction of biosensor to transduce and output signal. Currently, the bi-functional linkers can be classified into the following categories: (1) organic small molecules containing two functional groups. For example, *N*-succinimidyl 4-(maleimidome)cyclo-hexanecarboxylate (SMCC) contains *N*-hydroxysuccinimide ester and maleimide group, which can separately covalently bind with amine and sulfhydryl groups [1]. (2) Chemical group modified nucleic acid strand. For instance, bi-functional DNA probes modified with sulfhydryl groups at one end and alkynyl groups at the other end can be recognized by PSC@Au and azides through Au-S bond and click chemistry, respectively [2]. (3) Antibody/antigen-nucleic acid conjugates. The conjugates can simultaneously recognize the antigen/antibody and the complementary chain through antigen-antibody interaction and complementary base pairing, respectively [3]. The exploration of bi-functional linkers is of great importance for the development of a variety of analytical techniques.

✉ Qin Mi
rjhnmq@163.com

✉ Juan Zhang
juanzhang@shu.edu.cn

1 Shanghai Engineering Research Center of Food Microbiology, School of Health Science and Engineering, University of Shanghai for Science and Technology, Shanghai 200093, China

2 Center for Molecular Recognition and Biosensing, Joint International Research Laboratory of Biomaterials and Biotechnology in Organ Repair, Ministry of Education, Shanghai Engineering Research Center of Organ Repair, School of Life Sciences, Shanghai University, Shanghai 200444, China

3 Department of Food Science and Engineering, School of Agriculture and Biology, Shanghai Jiao Tong University, Shanghai 200240, China

4 Ruijin-Hainan Hospital Shanghai Jiaotong University School of Medicine (Hainan Boao Research Hospital), Shanghai, Hainan 570203, China

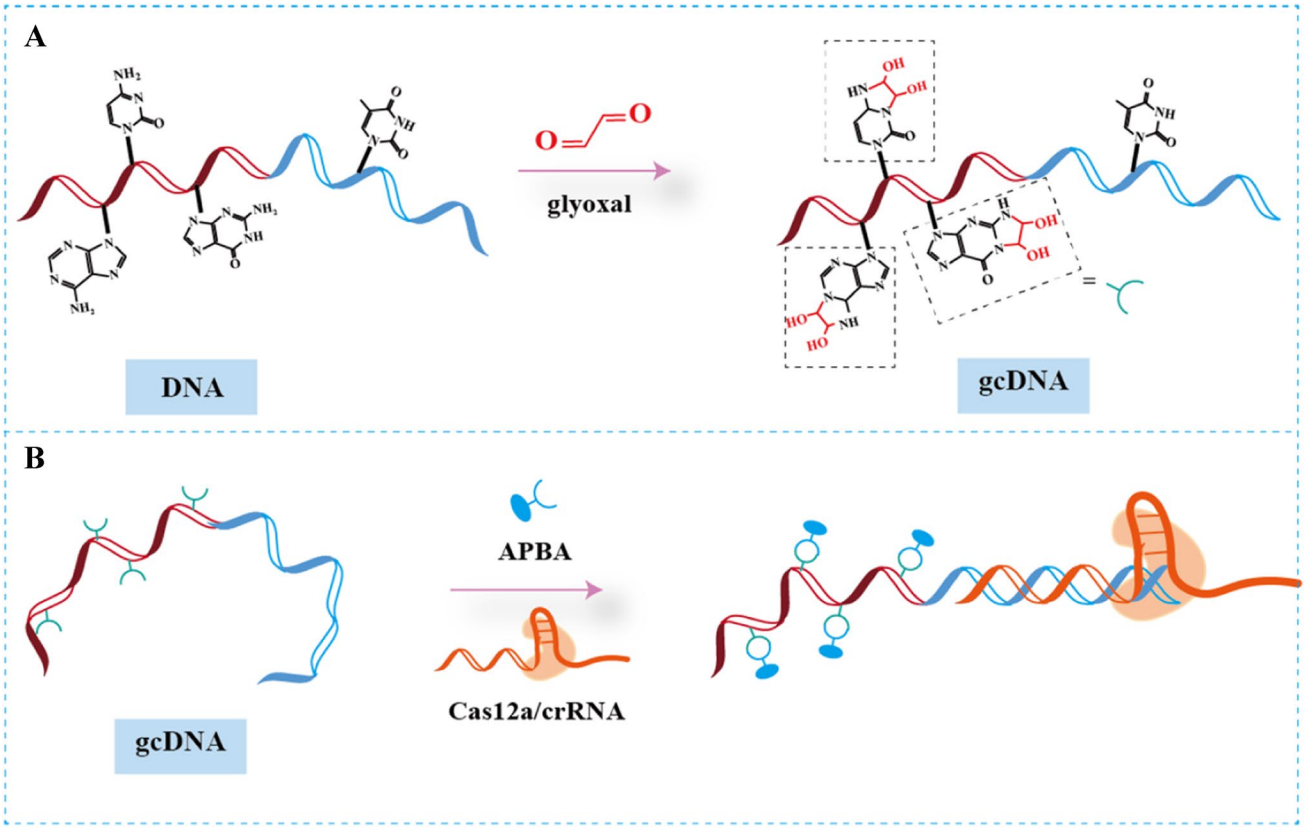


**Scheme 1** **A** Workflow of DNA reaction with glyoxal. **B** Bi-functional glyoxal caged DNA for simultaneous recognition by boronic acid and complementary DNA

Stable bis-hemiaminal adducts can be produced from the reaction between glyoxal and nitrogen groups on the Watson–Crick–Franklin face of nucleobases, resulting in the caging of nucleic acid [4, 5]. Due to the existence of diol groups in their molecular structure, these adducts can be theoretically recognized by boronic acid groups which can reversibly bind with 1,2-/1,3-*cis*-diols to form cyclic esters [6–9]. Moreover, the formation of these adducts will directly hinder complementary base-pairing and denature overall secondary structure [4, 10]. Interestingly, for four bases composed of nucleic acid, only guanosine, adenosine, and cytidine can react with glyoxal to form their additions, and, inversely, thymine cannot react due to the shortage of the corresponding nitrogen group in its molecular structure. Therefore, through programmatically rational design of its sequence with guanosine, adenosine, and cytidine bases on the one end and thymine bases on the other end, gcDNA will own bi-functionality for simultaneous boronic acid recognition and complementary base-pairing property.

In this work, DNA sequences consisting of glyoxal cage region, spacer region, and DNA complementary region were designed as recognition probes. The DNA sequence can react with glyoxal to obtain gcDNA, which can further be recognized by boronic acid groups and complementary bases (Scheme 1). Compared to the original DNA, we found that gcDNA exhibits excellent performance with boronic acid recognition and complementary base pairing. The bi-functional gcDNA is further coupled with CRISPR/Cas12a system for the establishment of new detection method of $Hg^{2+}$, with the aid of CMB@APBA. $Hg^{2+}$ can specifically cross-link with aminophenylboronic acid group surrounding CMB, thereby preventing the linkage of gcDNA onto CMB@APBA. In the absence of $Hg^{2+}$, CMB@APBA can react with gcDNA which can further bind with crRNA through complementary base pairing, resulting in the activation of CRISPR/Cas12a system and fluorescence signal output. Our established method has the following advantages: (1) With the aid of bi-functional gcDNA, CRISPR/Cas12a system can be efficiently activated to sensitively output the signal and realize the determination of trace $Hg^{2+}$. (2) The trace $Hg^{2+}$ in the sample matrix can be separated and preconcentrated by magnetic separation based on the specific reaction between boric acid groups and $Hg^{2+}$, to enhance the analytical specificity and sensitivity.

## Materials and methods

### Materials and reagents

The oligonucleotides used in the experiment were synthesized and purified by Sangon Biotech Co., Ltd (Shanghai, China), and their sequences are listed in Table S1. The carboxyl magnetic beads (CMB) were purchased from Invitrogen (Thermo Fisher Nicolet, USA). DEPC water was obtained from Sangon Biotech Co., Ltd (Shanghai, China). Lba Cas12a was obtained from Kexin Biomedical Technology Co., Ltd (Beijing, China). NEBuffer 2.1 was purchased from New England Biolabs, Inc. (Beijing, China). Methyl sulfoxide (DMSO), 40% glyoxal, 3-aminobenzeneboronic acid (APBA), Pb $(CH_3COO)_2$, $NiCl_2{\cdot}6H_2O$, $FeCl_2$, $HgCl_2$, $CrCl_3$, $ZnCl_2$, $MgCl_2$, and $CaCl_2$ were all analytical grade and bought from Sigma-Aldrich (Shanghai, China). 5 × loading buffer (including nucleic acid dye) was purchased from Shanghai Generay Biotech Co., Ltd (Generay, China). Milli-Q water (18.2 MΩ·cm) from a Milli-Q purification system (Milford, USA) was used in all experiments. Milk and tea drinks were purchased from local supermarket (Shanghai, China). Carboxyl polystyrene sphere (CPS, size ~ 1 μm) was received from Xi'an Qiyue Biotechnology Co., Ltd (China).

### Preparation of gcDNA and its reaction with APBA

gcDNA was prepared according to the reported method [4]. Briefly, 2 μL of the nucleic acid strands (100 μM) was mixed with 35 μL of 40% glyoxal and 50 μL DMSO, followed by the addition of DEPC water to give a final volume of 100 μL. The mixture was incubated at 50 °C for 40 min to give gcDNA. Subsequently, 2 μL of APBA solution (100 mg/mL) was added to the above gcDNA, and the mixture was adjusted by diluted HCl and then reacted at 37 °C for 1 h to give gcDNA/APBA. The gcDNA and gcDNA/APBA were loaded onto illustra MicroSpin G-25 Columns to remove the unreacted small impurities. The purified products were analyzed by mass spectrometry (MS) (LTQ XL, Thermo, America). At the same time, the products were characterized by 15% non-denaturing polyacrylamide gel electrophoresis (PAGE), and the gels were imaged by using a Gel Doc XR + Imaging System (Bio-Rad, USA).

### Recognition of gcDNA by CMB@APBA

Twenty microliters of prepared CMB@APBA (5 mg/mL) was separated through a magnet to remove the supernatant. The obtained precipitant was mixed with the FgcDNA (100 μL, 400 nM) and then reacted at 37 °C for 1 h. After washing twice with PBS to remove the unbound FgcDNA with the aid of a magnet, the obtained CMB@APBA/FgcDNA was analyzed by LSM 710 confocal laser scanning microscopy (Zeiss, Germany).

### Reaction of $Hg^{2+}$ with APBA and its capture by CMB@APBA

$HgCl_2$ was dissolved in ultrapure water to give the sample solution containing different concentrations of $Hg^{2+}$. Then, the sample solution (50 μL) was mixed with 2 μL APBA (100 mg/mL) and PBS to the final volume of 1 mL, and the mixture was incubated for 30 min at room temperature. The obtained products were measured by fluorescence spectrophotometer at an excitation wavelength of 300 nm and an emission wavelength of 375 nm. To study the capture of $Hg^{2+}$ by CMB@APBA, 20 μL $Hg^{2+}$ (800 μM) was added to the CMB@APBA (5 mg/mL). The mixture was incubated at room temperature for 30 min. Finally, the obtained products were characterized by Fourier transform infrared spectroscopy (FT-IR) (Vertex 70, Bruker, Germany), X-ray photoelectron spectroscopy (XPS) (AXIS Ultra DLD, Shimadzu, Japan), and scanning electron microscope (SEM) (GeminiSEM, ZEISS, Germany), respectively.

### Analysis of $Hg^{2+}$ through bi-functional gcDNA coupled with CRISPR/Cas12a system

Twenty microliters of $Hg^{2+}$ solutions with different concentrations was mixed with CMB@APBA (5 mg/mL), and the mixture was kept at room temperature for 30 min, to give CMB@APBA/$Hg^{2+}$. After magnetic separation, the supernatant was removed, and 100 μL of gcDNA was added, and the mixture was incubated at 37 °C for 1 h. After washing twice with DEPC, 3.2 μL of Cas12a (160 nM), 0.8 μL of crRNA (160 nM), 0.8 μL of ssDNA (1.6 μM), and 8 μL of NEBuffer 2.1 were added, followed by the addition of PBS (pH 7.4) to give a final volume of 100 μL. The mixture was reacted at 37 °C for 30 min, followed by heating at 65 °C for 10 min to inactivate Cas12a. After magnetic separation, the supernatant was analyzed by F-7000 fluorescence spectrophotometer (Hitachi Ltd., Japan) at an excitation wavelength of 480 nm and an emission wavelength of 520 nm, with the slits of excitation and emission at 10 nm and 10 nm, respectively.

### Validation of the method

The specificity of the established method was studied with 200 times higher concentrations of the interfering metal ions, including $Cr^{3+}$, $Ca^{2+}$, $Fe^{2+}$, $Mg^{2+}$, $Zn^{2+}$, $Ni^{2+}$, and $Pb^{2+}$ instead of $Hg^{2+}$. The 1 μM of $Hg^{2+}$ was replaced with 200 μM of other metal ions to evaluate the specificity. The selectivity of the established method was evaluated through

mixing the interfering ions with $Hg^{2+}$, together. To evaluate the applicability of the established method, milk and tea drinks were diluted 100 times with Milli-Q water and passed through a 0.45-μm filter membrane. Then, the different concentrations of $Hg^{2+}$ (40 nM, 100 nM, and 300 nM) were added to give the spiked samples. The concentrations of $Hg^{2+}$ in these samples were detected by the established method and inductively coupled plasma-mass spectrometry (ICP-MS), respectively.

## Results and discussion

### Synthesis of gcDNA and its binding with APBA

gcDNA with diol groups in its molecular structure has been synthesized, and their binding with boronic acid group has been deeply investigated. Glyoxal can react with adenine (A), guanine (G), and cytosine (C) bases of DNA to generate corresponding stable dihydroxy adducts (Fig. 1A) [4].

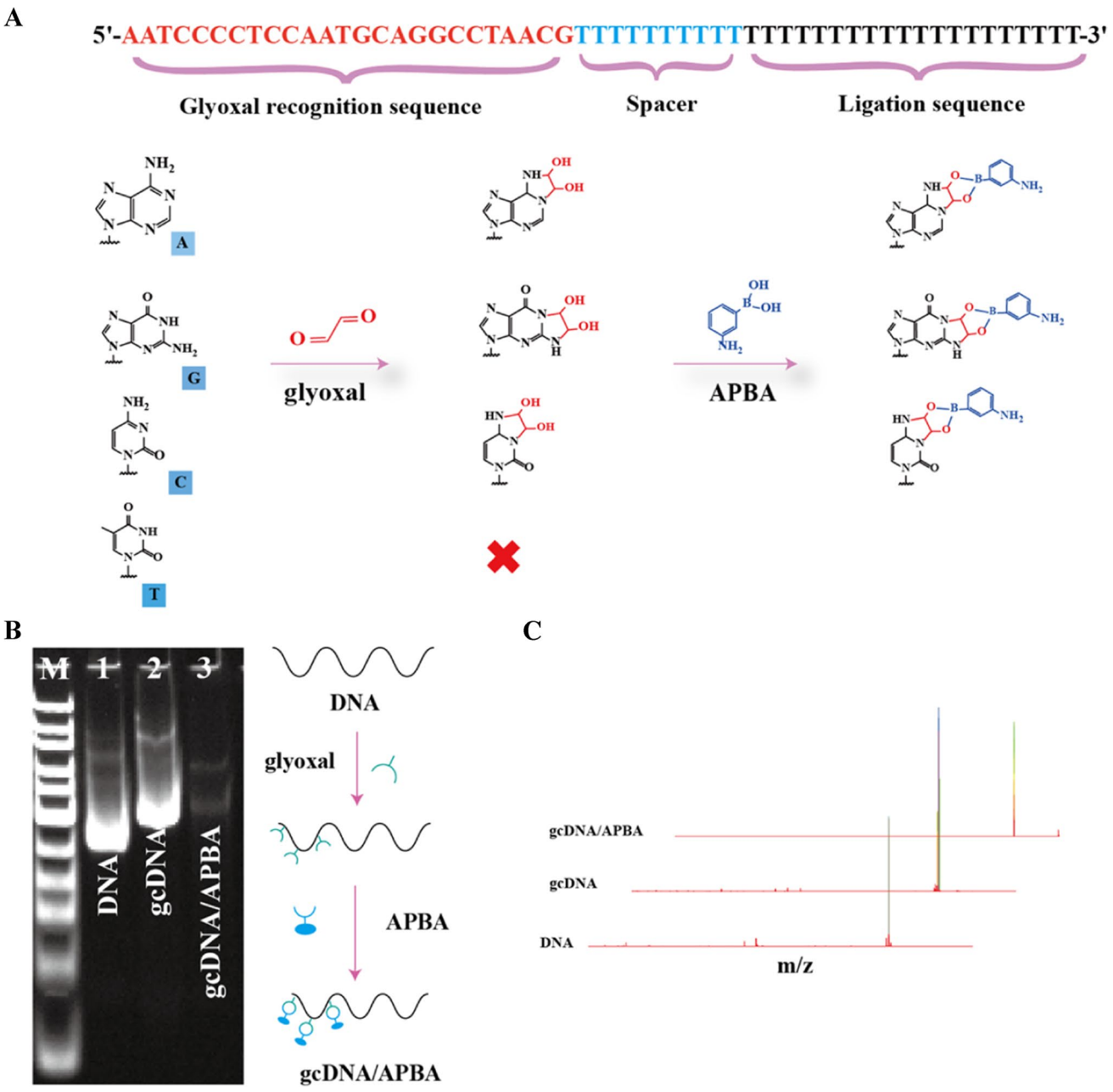


**Fig. 1** Synthesis of gcDNA and its binding with APBA. **A** The reaction of glyoxal with nucleobases and the reaction of bis-hemiaminal adducts with APBA. **B** 15% PAGE images of DNA, gcDNA, and gcDNA/APBA. **C** MS spectra of DNA, gcDNA, and gcDNA/APBA

As determined by MS measurements (Fig. 1C), gcDNA was successfully synthesized by the reaction between glyoxal and Watson–Crick–Franklin face of several nucleobases and then reacted with APBA to obtain gcDNA/APBA. Moreover, the high band (lane 2, Fig. 1B) can be found for gcDNA in comparison with that for DNA, which can be explained for low migration rate of gcDNA due to its large molecular weight. gcDNA/APBA exhibits the highest band (lane 3, Fig. 1B), due to its largest molecular weight among three substances. These results well verify the successful caging of DNA by glyoxal and its following successful recognition by APBA.

## gcDNA coupled with CRISPR/Cas12a system

Except for T base, other bases including A, G, and C bases can react with glyoxal, resulting in the formation of caged DNA and the loss of complementary base-pairing characteristics [10]. As exhibited in Fig. 2A, FgcDNA with dihydroxy groups of caged A, G, and C bases on one end and T bases on the other end can be simultaneously recognized by APBA and Cy3-labeled complementary DNA (FcDNA) through the formation of boronate ester and A-T base pairing, respectively. Compared with bands in lanes 1 and 2, the band in lane 3 can be attributed to the duplex gcDNA/cDNA. Meanwhile, similar band in lane 4 can be found with the further addition of APBA (Fig. 2B). The result well signifies that the formation of boronate ester bond between APBA and caged A, G, and C bases on one end of gcDNA has no impact on the binding of cDNA with gcDNA. Moreover, for mixture of FgcDNA and FcDNA, the new peak at 570 nm appears as a result of the formation of FgcDNA/FcDNA which shortens the distance between the fluorescence donor group Alexa488

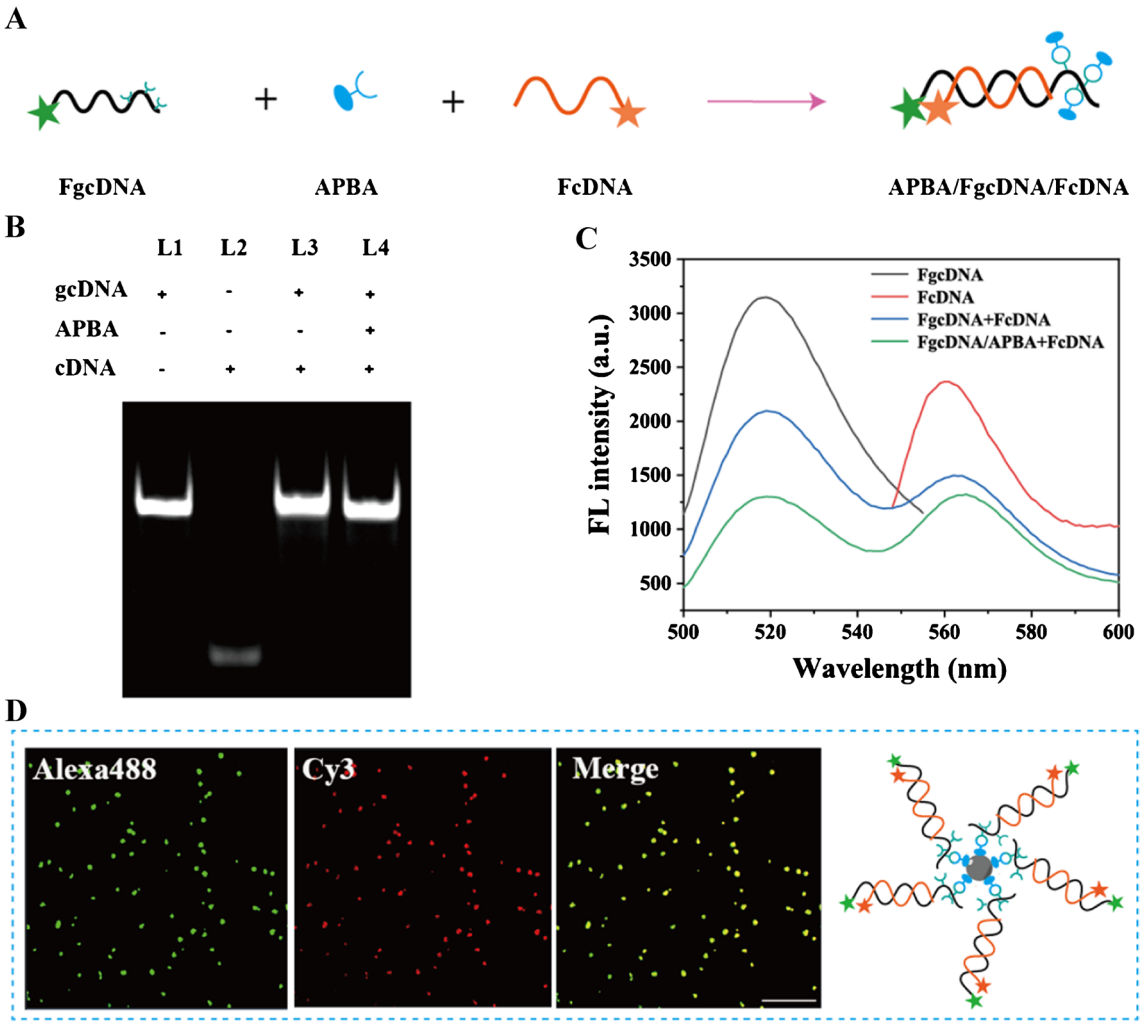


**Fig. 2** The bi-functionality of gcDNA. **A** Schematic illustration for the Alexa488-modified glyoxal caging DNA (FgcDNA) simultaneous recognized by APBA and FcDNA. **B** Polyacrylamide gel electrophoretic images. **C** Fluorescence spectra for FgcDNA simultaneously binding with APBA and FcDNA. **D** Laser confocal fluorescence images for FgcDNA simultaneous recognized by CMB@APBA and FcDNA (fluorescence intensity of FcDNA in supernatant). Scale bar: 10 μm

and acceptor group Cy3, so as to induce fluorescence resonance energy transfer (blue curve, Fig. 2C). The similar peak can be found with further addition of APBA (green curve, Fig. 2C), verifying almost no influence of APBA on the formation of FgcDNA/FcDNA. These results well confirm that rationally designed bi-functional FgcDNA has an ability to simultaneous bind with APBA and cDNA in the solution.

We further study the ability of gcDNA as a linker to immobilize cDNA onto the surface of CMB@APBA. As exhibited in Fig. 2D, green and red fluorescence can be observed, and the results well confirm that FgcDNA can link FcDNA onto the surface of CMB@APBA through the formed boronate ester bond and hydrogen bond between A and T bases. These results well suggest that gcDNA can be used as a bi-functional linker for the immobilization of cDNA onto solid interface.

It has been well known that complementary base pairing in duplex can induce the occurrence of many biological events. For example, the nuclease activity of clustered regularly interspaced short palindromic repeats/CRISPR-associated protein (CRISPR-Cas) system can be activated through complementary base pairing between activated strand and CRISPR RNA (crRNA) [14]. The activated CRISPR-Cas system owns the capability of efficiently indiscriminate cleavage on single-stranded DNA (ssDNA) and can serve for sensitive analysis of trace targets [11–14]. For instance, Lachnospiraceae bacterium ND2006 Cas12a–CRISPR RNA (CRISPR/LbCas12a) trans-cleaves ssDNA at approximately 3 turnovers per second with $k_{cat}/K_m$ value of $5.0\times10^6$ $s^{-1}$ $M^{-1}$ [15]. With complementary base-pairing functionality, the designed gcDNA can be developed to activate CRISPR-Cas12a system, so as to sensitively detect the trace targets. On the basis of bi-functional gcDNA as a linker, it has been further explored to activate CRISPR/Cas12a system (Fig. 3A). gcDNA/APBA can bind with crRNA through the complementary base pairing, so as to activate cis-cleavage and trans-cleavage activities by the RuvC catalytic pocket of Cas12a [16, 17]. As exhibited in Fig. 3B and Fig. S2, similar $k_{cat}/K_m$ values can be found for DNA ($4.67\times10^7$ $s^{-1}$ $M^{-1}$), gcDNA ($3.4\times10^7$ $s^{-1}$ $M^{-1}$), and gcDNA/APBA ($3.57\times10^7$ $s^{-1}$ $M^{-1}$), respectively. These results well suggest that the introduction of boronic acid recognition does not affect the activated effect of the gcDNA on CRISPR/Cas12a system and its corresponding trans-cleavage activity.

The activation effect of gcDNA/APBA immobilized on the interface has been further investigated. After activation of CRISPR/Cas12a system, *cis*-cleavage firstly happens to cleave the 22nd base of gcDNA/APBA, counting from the first 3′-base that was paired with the crRNA guide sequence [17], leading to the departure of activated CRISPR/Cas12a system from CMB interface into the solution (Fig. 3C and Fig. S3). The majority of the crRNA/Cas12a complex most likely remains bound to the residual gcDNA/APBA after cis-cleavage, protecting the binding section of gcDNA/APBA from exposing the trans-cleavage sites of the Cas12a ternary complex [17]. Under the spacer length of 20 nt (Fig. S1(F)), a similarly low value of $k_{cat}/K_m$ value ($1.65\times10^7$ $s^{-1}$ $M^{-1}$) can be observed for CRISPR/Cas12a system activated by CPS@APBA/gcDNA (Fig. 3D and Fig. S4), compared with gcDNA ($3.4\times10^7$ $s^{-1}$ $M^{-1}$) and gcDNA/APBA ($3.57\times10^7$ $s^{-1}$ $M^{-1}$).

## Capture and enrichment of $Hg^{2+}$ by CMB@APBA

Due to the complex food matrix and low amount, the determination of $Hg^{2+}$ in food samples faces great challenges. As a kind of functional material, magnetic beads have the advantages of easy modification, separation, and enrichment [18–20] and can well be applied for capture of metal ions in complicated food samples. The synthesized CMB@APBA can selectively react with $Hg^{2+}$, resulting in the substitution of B atom around CMB by Hg atom (Fig. 4A). As shown in Fig. 4B, the peaks at 1631 $cm^{-1}$ could be assigned to the stretching vibration of C-N, which confirms the successful modification of CMB by APBA through amide bond [21, 22]. Moreover, the disappearance of peak at 1405 $cm^{-1}$ attributed to the stretching vibration of B-O bond [23] and the other peak at 1074 $cm^{-1}$ for the stretching vibration of C-B bond [24] and the appearance of new absorbance peak at 1450 $cm^{-1}$ for C-Hg bond verify that the successful trans-metalation reaction between $Hg^{2+}$ and phenylboronic acid [25, 26]. As exhibited in Fig. 4C, the formed CMB@APBA/$Hg^{2+}$ is spherical with a rough surface which can be attributed for the modification of APBA and the subsequent substitution of Hg [27]. It can be found the existence and uniform distribution of C, N, and Hg around magnetic bead (Fig. 4C). Besides, as displayed in Fig. 4D, the peaks of O 1 s, N 1 s, and C 1 s 4f appeared at 531.2, 399.7, and 284.7, respectively, and the two characteristic peaks at 100.6 eV and 104.6 eV can be assigned to Hg $4f_{7/2}$ and Hg $4f_{5/2}$ of $Hg^{2+}$, confirming the successful capture of $Hg^{2+}$ on the CMB@APBA [28].

## The determination of $Hg^{2+}$ through fluorescence method based on gcDNA coupled with CRISPR/Cas12a system and its performance evaluation

Bi-functional gcDNA coupled with CRISPR/Cas12a system has been explored for fluorescence method to detect $Hg^{2+}$ with the assistance of CMB@APBA. As exhibited in Fig. 5, in the absence of $Hg^{2+}$, gcDNA can bind with aminophenylboronic acid group around CMB@APBA to form CMB@APBA/gcDNA through the ester bond. The exposed sequence consisting of only T bases can activate CRISPR/Cas12a system to indiscriminately cleave the ssDNA, leading to fluorescence recovery. In the presence of $Hg^{2+}$, it can

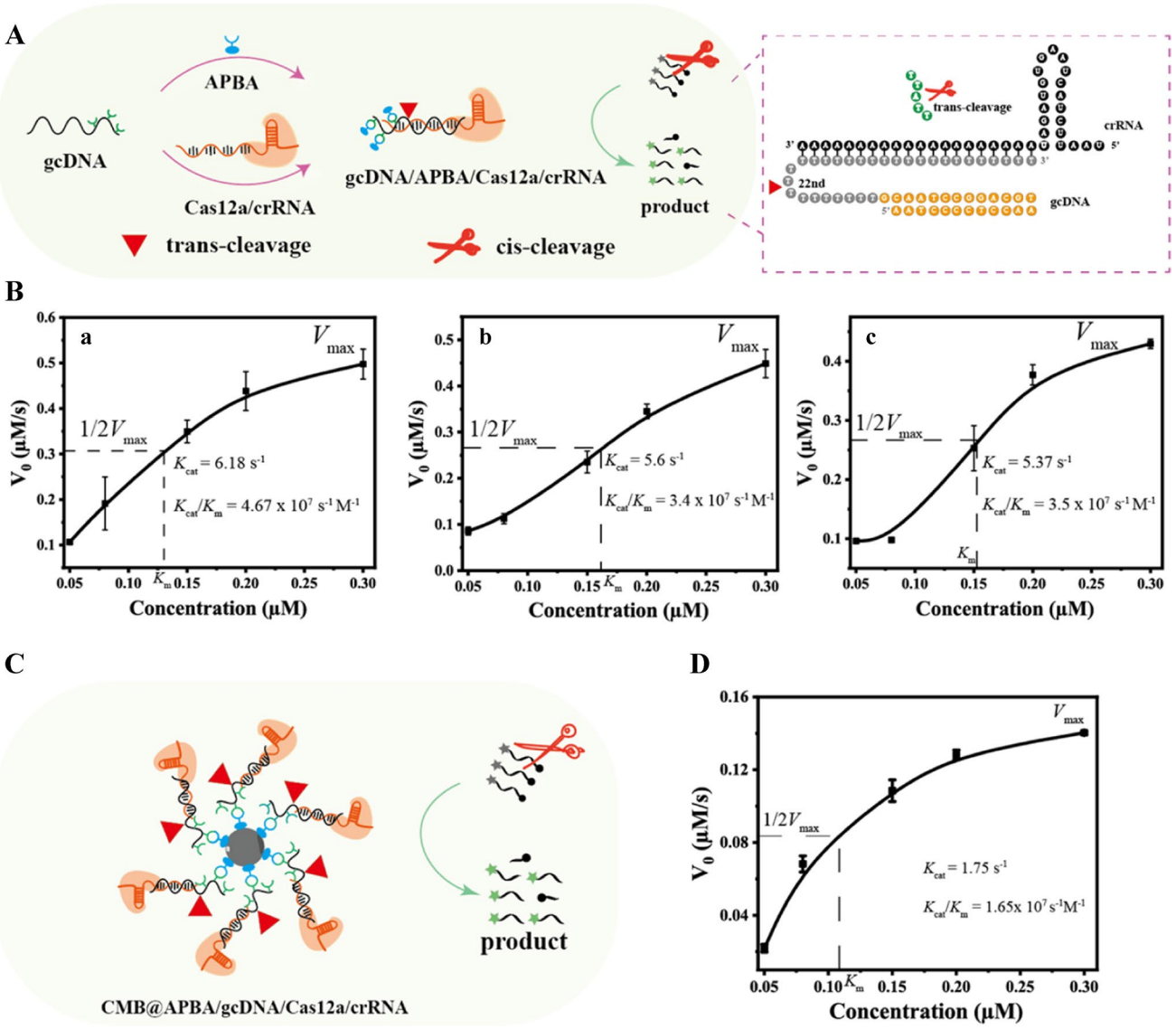


**Fig. 3** Bi-functional gcDNA coupled with CRISPR/Cas12a system. **A** Scheme illustration for the activation of Cas12a/crRNA system by gcDNA/APBA. **B** Michaelis-Menten kinetic study for (a) DNA, (b) gcDNA, and (c) gcDNA/APBA-activated Cas12a/crRNA system. **C** Scheme illustration for CMB@APBA/gcDNA-activated Cas12a/crRNA system. **D** Michaelis-Menten plot for CPS@APBA/gcDNA-activated Cas12a/crRNA system. Error bars represent the standard deviation of three experiments

react specifically with CMB@APBA, thereby preventing the binding of gcDNA.

Under the optimal experimental conditions (Fig. S1), including pH value (6.0), the concentration of gcDNA (400 nM), and the spacer length of gcDNA (20 nt), the constructed fluorescence method has been utilized to quantitatively detect $Hg^{2+}$. As shown in Fig. 6A, the fluorescence intensity at 520 nm gradually decreases as the $Hg^{2+}$ concentration increases from 0 to 4000 nM. The increased $Hg^{2+}$ will cause more trans-metalation reaction with aminophenylboronic acid groups around CMB@APBA, resulting in the reduction of boronic acid groups and the binding of a decreased amount of gcDNA. Almost no fluorescence can be observed with the concentration of $Hg^{2+}$ at 1 μM, as a result of the total reaction of boronic acid groups at the surrounding of CMB@APBA. The fluorescence intensity at 520 nm has been further used for quantitative analysis of $Hg^{2+}$. It can be observed that the fluorescence intensity at 520 nm is inversely proportional to the logarithmic values of $Hg^{2+}$ concentrations in the range of 20–250 nM (Fig. 6B). A linear equation of $I = -528.276\,\mathrm{Log}C_{Hg2+} + 1920.057$ can be obtained with a lowest limit of detection of 2.72 nM (S/N = 3), about 500 times lower than the above fluorescence method (0.85 μM) and colorimetric method (1.40 μM) (Fig. S5). Moreover, compared with the reported methods, the developed

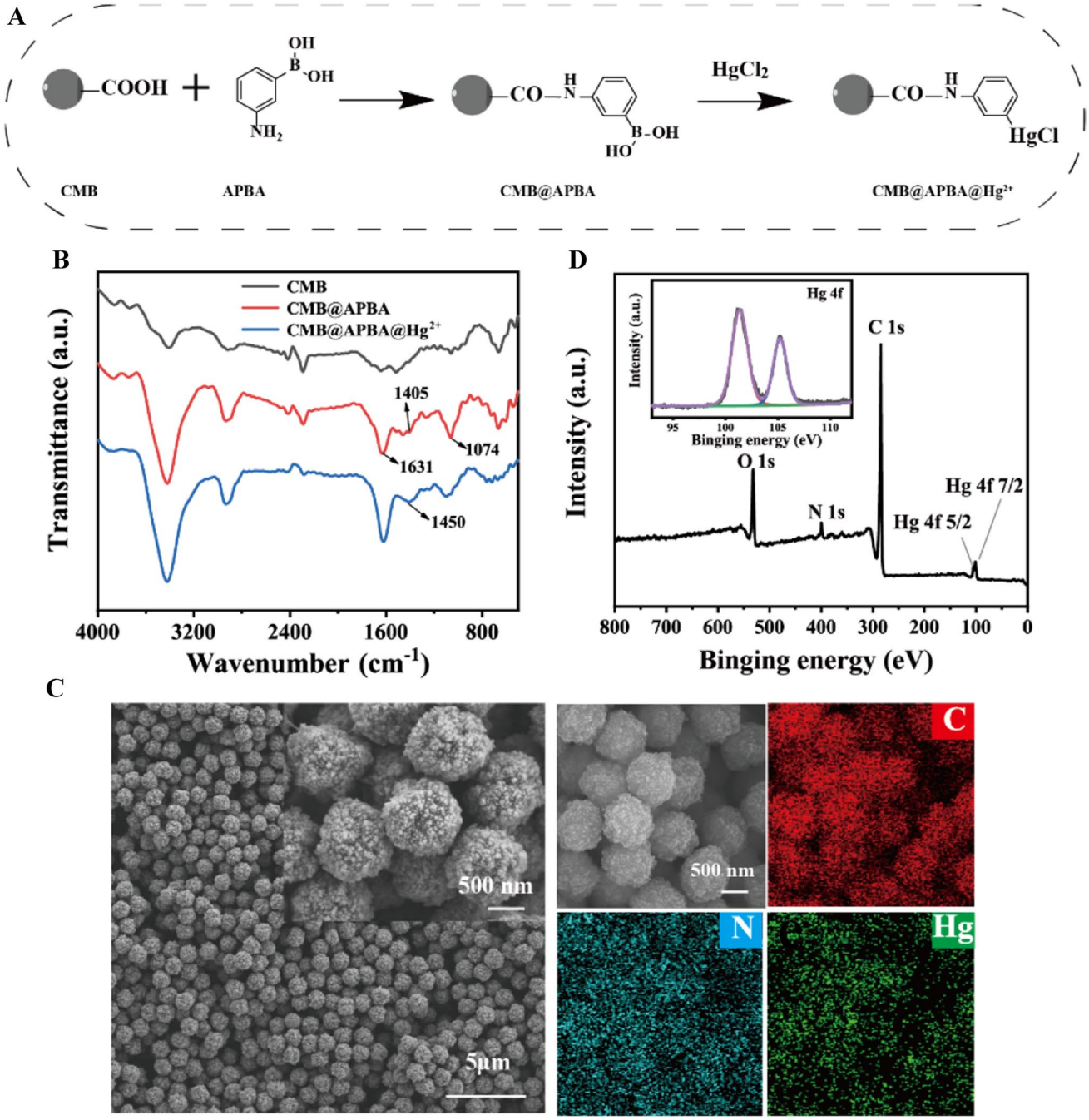


**Fig. 4** Capture and enrichment of $Hg^{2+}$ by CMB@APBA. **A** Schematic illustration for the capturing of $Hg^{2+}$ by CMB@APBA. **B** FIRT spectra of CMB, CMB@APBA, and CMB@APBA/$Hg^{2+}$. **C** SEM images and elemental mapping of CMB@APBA/$Hg^{2+}$. **D** XPS survey spectrum of CMB@APBA/$Hg^{2+}$. Inset: XPS component peak-fitting spectra of Hg 4f

fluorescence method exhibits a low LOD, demonstrating its good sensitivity (Table S3).

The specificity of the established fluorescence method has been evaluated by using 200 times concentrations of other ions instead of $Hg^{2+}$ (Fig. 6C). The low fluorescence intensity can be only found for $Hg^{2+}$, due to its specific reaction with aminophenylboronic acid around CMB@APBA [29]. Inversely, potentially interfering ions exhibit the high fluorescence intensity because these ions cannot react with aminophenylboronic acid. The selectivity has been further investigated through mixing 200 times high concentration of potentially interfering ions with $Hg^{2+}$. No statistic difference can be found for $Hg^{2+}$ in comparison with all mixtures (Fig. 6D), signifying that

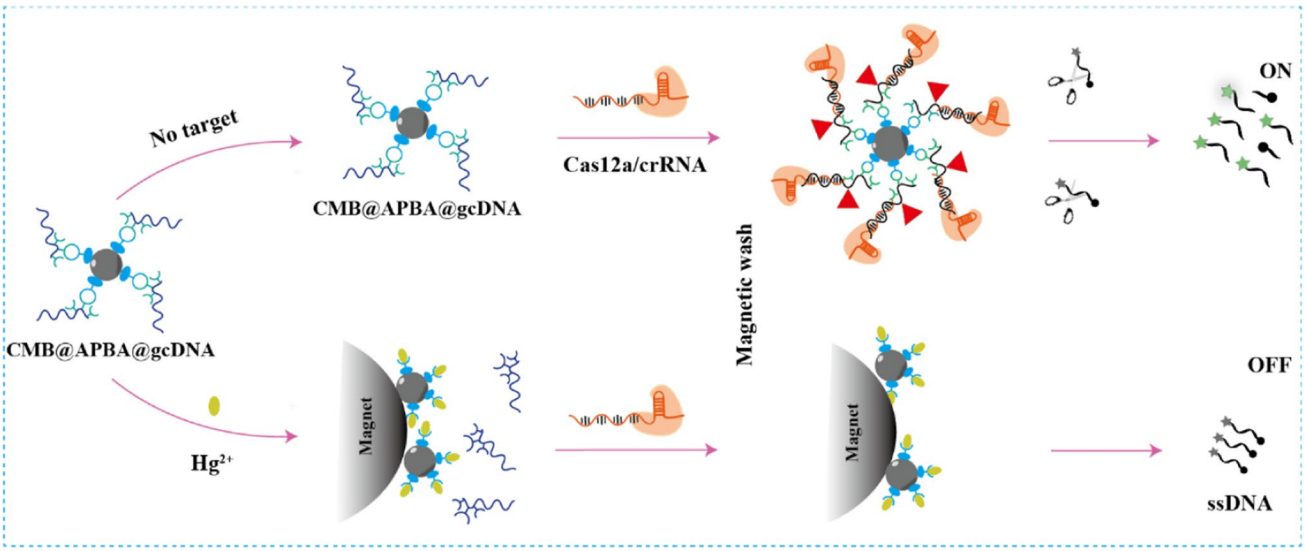


**Fig. 5** Schematic illustration of the determination of $Hg^{2+}$ through fluorescence method based on bi-functional gcDNA coupled with CRISPR/Cas12a system

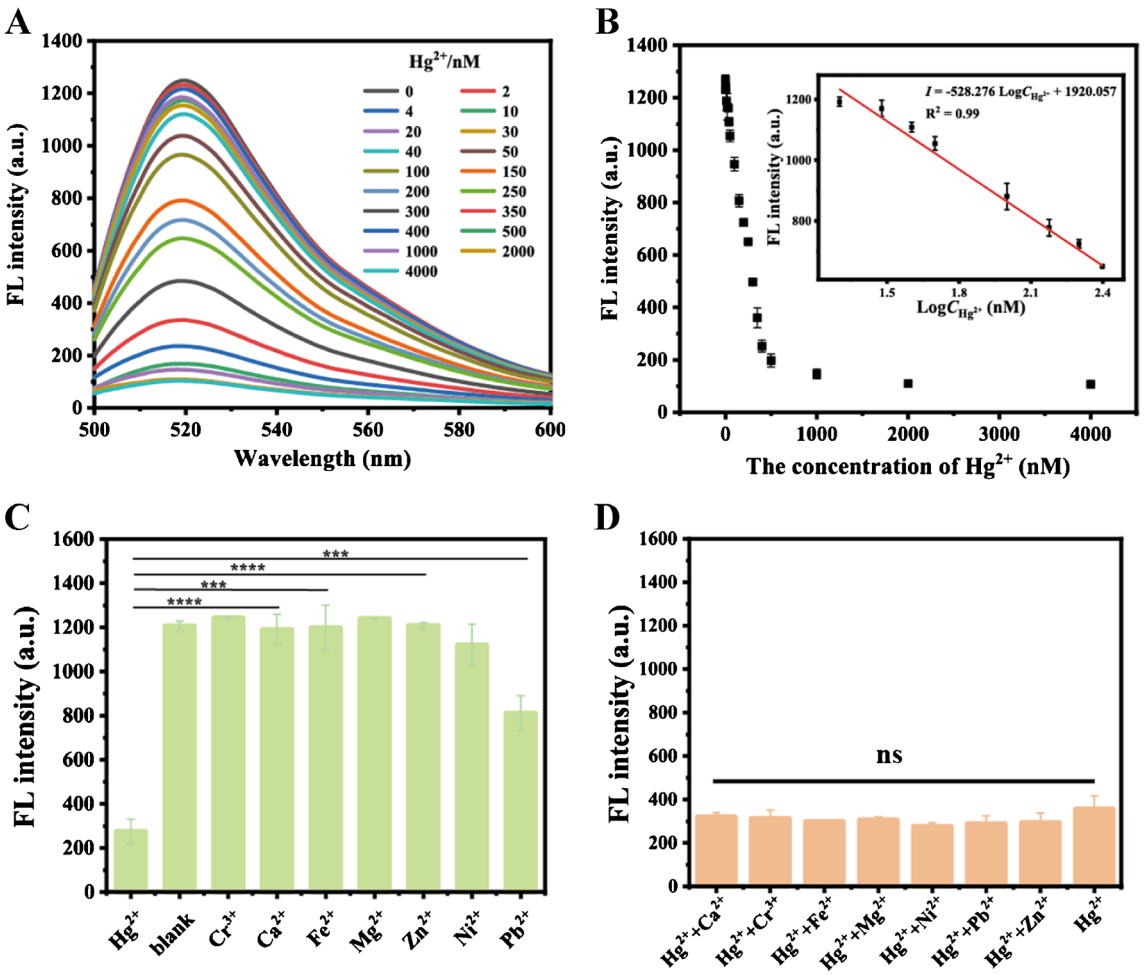


**Fig. 6** **A** Fluorescence spectra obtained with different concentrations of $Hg^{2+}$. **B** The fluorescence intensity versus $Hg^{2+}$ concentration. Inset: The linear relationship between the fluorescence intensity at 520 nM and the logarithm of $Hg^{2+}$ concentration. **C** Specificity and **D** selectivity of fluorescence method for $Hg^{2+}$ analysis. The concentration of $Hg^{2+}$ and other metal ions was 1 μM and 200 μM, respectively

other ions have no influence on the reaction between $Hg^{2+}$ and aminophenylboronic acid.

Finally, the practicability of the fluorescence method has been investigated by analyzing the 1000 times diluted certified mercury ion standard solution (1 mg/L mercury standard solution (GSB04-1729–2004)). As shown in Table S4, the detected value in agreement with the standard values signifies that the established fluorescence method can be used for the determination of $Hg^{2+}$. The complicated matrix of food sample contaminated by trace $Hg^{2+}$ provides great challenge on the performance of the fluorescence method [30]. Taking the spiked dairy products and tea beverages as examples, we evaluate the practicability of the developed fluorescence method. As exhibited in Fig. S6 (A) and (B), the recovery ratios of 101.63 ~ 114.73% and 100.87 ~ 112.97% can be obtained with RSD values of 9.59% and 10.49% for tea beverages and dairy products, respectively. Furthermore, the spiked samples with different concentrations of $Hg^{2+}$ in dairy products and tea beverages have also been detected by the ICP-MS. As shown in Fig. S6 (C) and (D), there was no statistical difference between the $Hg^{2+}$ concentration detected by the established fluorescence method and those measured by ICP-MS. The results show that the fluorescence method can be used for the determination of $Hg^{2+}$ in complicated food samples. These can be attributed to the specific capture of CMB@APBA on $Hg^{2+}$ and the subsequent magnetic separation to eliminate the interference of complicated sample matrix.

## Conclusion

In conclusion, gcDNA has been firstly explored as a bifunctional linker to bind with phenylboronic acid group and complementary DNA/RNA, through rational designation with guanosine, adenosine, and cytidine bases on the one end and thymine bases on the other end. For gcDNA, glyoxal caged guanosine, adenosine, and cytidine bases with diol groups can react with boronic acid group around magnetic bead with a maximized coverage density of $2.1 \times 10^5$ $\mu m^{-2}$ under acidic condition, while thymine bases can further quantitatively bind with complementary RNA through U-T base pairing. Coupling with CRISPR/Cas12a system, gcDNA has been further developed for the determination of $Hg^{2+}$ by using its specific cross-metal reaction with phenylboronic acid group. Through magnetic separation to efficiently capture and enrich $Hg^{2+}$ from complicated food matrix, the method exhibits good specificity, selectivity, and practicability, with the LOD of 2.72 nM, about 500 times lower than the corresponding fluorescence method (0.85 μM) and colorimetric method (1.40 μM). In conclusion, the structure characteristic of gcDNA is crucial for the method and should be taken into account when generalized to other method supported by the interface.

**Supplementary Information** The online version contains supplementary material available at https://doi.org/10.1007/s00604-024-06196-5.

**Author contribution** Juan Zhang: conceived the project; Ying Yu: designed and coordinated the experiments; Ying Yu, Yuan Zhang, and Lelin Qian: performed experiments; Ying Yu, Wenhui Li, and Qin Mi: analyzed results; Ying Yu and Juan Zhang: wrote the manuscript; and Juan Zhang and Zhengwu Wang: funding acquisition. All authors reviewed and commented on the manuscript.

**Funding** This work is sponsored by the Special National Key Research and Development Plan (Grant No. 2018YFC160440), the Science and Technology Commission of Shanghai Municipality (Grant No. 20392001800), and the National Natural Science Foundation of China (Grant No. 31671923).

**Data availability** The data that support the findings of this study are available from the corresponding author, upon reasonable request.

## Declarations

**Conflict of interest** The authors declare no competing interests.

## References

1. Guo Y, Werbel T, Wan S et al (2016) Potent antigen-specific immune response induced by infusion of spleen cells coupled with succinimidyl-4-(N-maleimidomethyl cyclohexane)-1-carboxylate (SMCC) conjugated antigens. Int Immunopharmacol 31:158–168. https://doi.org/10.1016/j.intimp.2015.12.023
2. Qing M, Xie S, Cai W et al (2018) Click chemistry reaction-triggered 3D DNA walking machine for sensitive electrochemical detection of copper ion. Anal Chem 90(19):11439–11445. https://doi.org/10.1021/acs.analchem.8b02555
3. Cao Y, Yu X, Han B et al (2021) In situ programmable DNA circuit-promoted electrochemical characterization of stemlike phenotype in breast cancer. J Am Chem Soc 143(39):16078–16086. https://doi.org/10.1021/jacs.1c06436
4. Knutson SD, Sanford AA, Swenson CS et al (2020) Thermoreversible control of nucleic acid structure and function with glyoxal caging. J Am Chem Soc 142(41):17766–17781. https://doi.org/10.1021/jacs.0c08996
5. Chen HJC, Chang YL, Teng YC et al (2017) A stable isotope dilution nanoflow liquid chromatography tandem mass spectrometry assay for the simultaneously detection and quantification of glyoxal-induced DNA cross-linked adducts in leukocytes from diabetic patients. Anal Chem 89(24):13082–13088. https://doi.org/10.1021/acs.analchem.6b04296
6. Otsuka H, Uchimura E, Koshino H et al (2004) Anomalous binding profile of phenylboronic acid with N-acetylneuraminic acid (Neu5Ac) in aqueous solution with varying pH. J Am Chem Soc 125(12):3493–3502
7. Zhang J, Liu Y, Wang X et al (2015) Electrochemical assay of α-glucosidase activity and the inhibitor screening in cell medium. Biosens Bioelectron 74:666–672. https://doi.org/10.1016/j.bios.2015.07.023
8. Zhang J, Lv J, Wang X et al (2015) Integration of chemoselective ligation with enzymespecific catalysis: saccharic colorimetric analysis using aminooxy/hydrazine-functionalized gold

nanoparticles. Nano Res 8:3853–3863. https://doi.org/10.1007/s12274-015-0885-9
9. Zhang J, Liu Y, Lv J, Li G (2015) A colorimetric method for α-glucosidase activity assay and its inhibitor screening based on aggregation of gold nanoparticles induced by specific recognition between phenylenediboronic acid and 4-aminophenyl-α-d-glucopyranoside. Nano Res 8:920–930. https://doi.org/10.1007/s12274-014-0573-1
10. Kaback DB, Angerer LM, Davidson V (1980) Improved methods for the formation and stabilization of R-loops. Nucleic Acids Res 12(21):8235–8251
11. Cheng L, Yang F, Tang L et al (2022) Electrochemical evaluation of tumor development via cellular interface supported CRISPR/Cas trans-cleavage. Research. https://doi.org/10.34133/2022/9826484
12. Zhang J, Sheng A, Wang P et al (2021) Mxene coupled with crispr-cas12a for analysis of endotoxin and bacteria. Anal Chem 93(10):4676–4681. https://doi.org/10.1021/acs.analchem.1c00371
13. Yu Y, Li W, Gu X et al (2022) Inhibition of CRISPR-Cas12a trans-cleavage by lead (II)-induced G-quadruplex and its analytical application. Food Chem 378:131802. https://doi.org/10.1016/j.foodchem.2021.131802
14. Zhu Y, Zhu J, Gao Y et al (2023) Electrochemical determination of flap endonuclease 1 activity amplified by CRISPR/Cas12a trans-cleavage**. ChemElectroChem 10(8):e202300020. https://doi.org/10.1002/celc.202300020
15. Chen JS, Ma E, Harrington LB et al (2018) CRISPR-Cas12a target binding unleashes indiscriminate single-stranded DNase activity. Science 360(6387):436–439. https://doi.org/10.1126/science.aar6245
16. Stella S, Mesa P, Thomsen J et al (2018) Conformational activation promotes CRISPR-Cas12a catalysis and resetting of the endonuclease activity. Cell 175(7):1856–1871. https://doi.org/10.1016/j.cell.2018.10.045
17. Li SY, Cheng QX, Liu JK et al (2018) CRISPR-Cas12a has both cis- and trans-cleavage activities on single-stranded DNA. Cell Res 28(4):491–493. https://doi.org/10.1038/s41422-018-0022-x
18. Dehghani Z, Nguyen T, Golabi M et al (2021) Magnetic beads modified with Pt/Pd nanoparticle and aptamer as a catalytic nanobioprobe in combination with loop mediated isothermal amplification for the on-site detection of Salmonella typhimurium in food and fecal samples. Food Control 121:107664. https://doi.org/10.1016/j.foodcont.2020.107664
19. Yang S, Ouyang H, Su X et al (2016) Dual-recognition detection of Staphylococcus aureus using vancomycin-functionalized magnetic beads as concentration carriers. Biosens Bioelectron 78:174–180. https://doi.org/10.1016/j.bios.2015.11.041
20. Deng M, Li W, Chen Y et al (2022) Detection of fumonisin B1 by aptamer-functionalized magnetic beads and ultra-performance liquid chromatography. Microchem J 178:107346. https://doi.org/10.1016/j.microc.2022.107346
21. Li S, Qin Y, Zhong G et al (2018) Highly efficient separation of glycoprotein by dual-functional magnetic metal-organic framework with hydrophilicity and boronic acid affinity. ACS Appl Mater Interfaces 10(33):27612–27620. https://doi.org/10.1021/acsami.8b07671
22. Wang Z, Liu J, Chen G et al (2022) An integrated system using phenylboronic acid functionalized magnetic beads and colorimetric detection for Staphylococcus aureus. Food Control 133:108633. https://doi.org/10.1016/j.foodcont.2021.108633
23. Feng S, Zhang A, Wu F et al (2022) In-situ growth of boronic acid-decorated metal-organic framework on $Fe_3O_4$ nanospheres for specific enrichment of cis-diol containing nucleosides. Anal Chim Acta 1206:339772. https://doi.org/10.1016/j.aca.2022.339772
24. Zou WS, Ye CH, Wang YQ et al (2018) A hybrid ratiometric probe for glucose detection based on synchronous responses to fluorescence quenching and resonance light scattering enhancement of boronic acid functionalized carbon dots. Sens Actuators B Chem 271:54–63. https://doi.org/10.1016/j.snb.2018.05.115
25. Chatterjee A, Banerjee M, Khandare DG et al (2017) Aggregation-induced emission-based chemodosimeter approach for selective sensing and imaging of Hg(II) and methylmercury species. Anal Chem 89(23):12698–12704. https://doi.org/10.1021/acs.analchem.7b02663
26. Wang H, Wang X, Liang M et al (2020) A boric acid-functionalized lanthanide metal-organic framework as a fluorescence "turn-on" probe for selective monitoring of $Hg^{2+}$ and $CH_3Hg^+$. Anal Chem 92(4):3366–3372. https://doi.org/10.1021/acs.analchem.9b05410
27. Hajri AK, Jamoussi B, Albalawi AE et al (2022) Designing of modified ion-imprinted chitosan particles for selective removal of mercury (II) ions. Carbohydr Polym 286:119207. https://doi.org/10.1016/j.carbpol.2022.119207
28. Yang J, Zhang Y, Guo J et al (2020) Nearly monodisperse copper selenide nanoparticles for recognition, enrichment, and sensing of mercury ions. ACS Appl Mater Interfaces 12(35):39118–39126. https://doi.org/10.1021/acsami.0c09865
29. Guo X, Huang J, Wei Y et al (2020) Fast and selective detection of mercury ions in environmental water by paper-based fluorescent sensor using boronic acid functionalized $MoS_2$ quantum dots. J Hazard Mater 381:120969. https://doi.org/10.1016/j.jhazmat.2019.120969
30. Behbahani M, Bide Y, Salarian M et al (2014) The use of tetragonal star-like polyaniline nanostructures for efficient solid phase extraction and trace detection of Pb(II) and Cu(II) in agricultural products, sea foods, and water samples. Food Chem 158:14–19. https://doi.org/10.1016/j.foodchem.2014.02.110